EXPERIMENTAL EVIDENCE FOR METALLURGICAL MODIFICATION ASSOCIATED TO CHUNKY GRAPHITE IN HEAVY-SECTION DUCTILE IRON CASTINGS

J. Lacaze
CIRIMAT, Université de Toulouse, Toulouse, France

I. Asenjo, S. Méndez, J. Sertucha, P. Larrañaga and R. Suárez
Engineering and Foundry Department, Azterlan, Durango (Bizkaia), Spain

Abstract

Heavy-section castings made of spheroidal graphite cast irons are known to be prone to graphite degeneracy. Upon the various degenerate forms of graphite reported in the literature, chunky graphite is the most common and detrimental one. A great deal of effort has been made for many years to prevent its formation but no convincing description of the factors controlling its appearance has been given so far.

In large-size castings, chunky graphite generally appears away from the surface and its occurrence is made evident on a metallographic section by a darker contrast. Because of this sharp and clear transition between the non-affected and the affected zones, several authors looked for chemical heterogeneities at the scale of the part but all concluded to the absence of macrosegregation.

This paper presents experimental evidence based on differential thermal analyses that metallurgical differences do exist in samples machined out of the affected and non-affected zones of a single cast block.

Keywords: *cast iron, heavy section, graphite degeneracy, chunky graphite*

Introduction

Heavy-section castings made of spheroidal graphite cast irons are known to be prone to graphite degeneracy.[1] Upon the various degenerate forms of graphite reported in the literature, chunky graphite (hereafter denoted as CHG) is the most common and detrimental. A great deal of effort has been made to prevent its formation and it has been found that use of chills as well as minute additions of Sb are amongst the most efficient.[2] Both actions have however their own drawbacks, chills being limited to sections a few centimetres thick while the addition of Sb (and other "counter-active" elements) is complicated because the necessary amount lies in a window that depends on the casting section and on other trace elements present and because Sb is a pearlite promoter.

CHG is a degenerate form of graphite that is mainly observed in the thermal centre of large spheroidal graphite (SG) castings,[3-5] but may also appear in thin sections of ductile iron castings containing high Ce and Si contents,[6] besides austenitic Ni-alloyed cast irons.[7] In large-size castings, CHG appears away from the surface and its formation becomes clear on metallographic sections by a darker contrast as illustrated in Figure 1. Numerous attempts have been made to describe the metallurgical process leading to the formation of CHG, but no convincing theory has been established until now. Because of the sharp and clear transition seen in Figure 1 between the non-affected and the affected zones, several authors looked for chemical heterogeneities but all concluded to the absence of macrosegregation.[8-11] It should be recognized however that the analysis methods used are obscured by detection limits and accuracies that are not always clearly stated. Moreover, they all estimate global compositions and are not able to differentiate if a particular species exists in an atomic state or bound within a compound.

This paper presents differential thermal analysis (DTA) experiments performed on samples machined from affected and non-affected zones of a single cast block. The DTA records show that there are in fact metallurgical differences between these two zones.

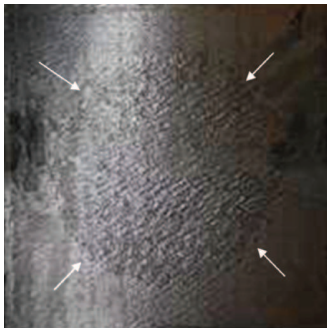

Figure 1. Photograph of the whole axial section of a cubic block 30 cm in size. The white arrows show the limit between the outer non-affected zone and the inner with-CHG area.

Experimental Investigation

Experimental Details

A cubic block 30 cm in size was cast following a procedure detailed previously.[12] The composition of the material as analyzed after casting was 3.68% C, 2.20% Si, 0.09% Mn, 0.035% P, 0.014% S, 0.040% Mg, 0.02% Cu, 0.005% Ti, 0.02% Cr, 0.011% V, 0.0123% Ce, 0.002% La (contents expressed in weight). Subsequent analyses made on an area with CHG graphite and another free of this defect did not show any chemical differences. According to a previous evaluation of the effect of various elements on the austenite and graphite liquidus,[13] this alloy is slightly hypoeutectic (carbon equivalent at 4.30%), the austenite liquidus temperature is 1167.6C (2133.7F) and the equilibrium eutectic temperature is 1158.3C (2116.9F). The micrographs in Figure 2 present the microstructure in the outer non-affected area (Figure 2-a) and in the inner zone (Figure 2-b). In this latter, several CHG cells are clearly visible. The central area affected with CHG (see Figure 1) amounts to 17.6% of the whole volume of the block, while the specific surface of CHG cells is as high as A_A = 25.0% in the central part.

Samples for DTA were machined in the outer area free of CHG (labelled no-CHG in the following) and from the centre (labelled with-CHG). The study specimens were cylinders 3.9 mm in diameter and 4 to 5 mm in length. The DTA experiments were designed to look for any differences in the cooling records that could be related to the origin of the samples, either with-CHG or no-CHG. Two series of trials were performed with one new sample for each run:

- heating to 1200C (2192F), holding 1800 sec. then cooling at either 2.5, 5, 10 or 20ºK/min;
- heating to 1200C (2192F), holding 1 sec. then cooling at 5, 10 or 15ºK/min (in this latter case, the upper temperature of the heating stage was increased to 1225C (2237F) in order to ensure complete melting of the sample before cooling starts).

In the first series of trials, the lengthy holding in the liquid state was designed so as to lead to full Mg fading and solidification with lamellar graphite. On the contrary, the trials with very rapid melting and short stay in the liquid state were expected to preserve alloy composition as much as possible. One additional trial consisted in applying a rapid melting and solidification at 10ºK/min down to 1000C (1832F), then reheating at 1200C (2192F) and holding 1800 sec., finally solidifying at 10º K/min. This trial was defined for reproducibility checking.

Independent calibration of the DTA cell with pure aluminium and nickel showed that it underestimated temperatures by about 3C. All records presented in the following have been corrected accordingly.

Results

The graphs in Figure 3 show the whole series of DTA records obtained upon cooling after sufficient time has been spent in the liquid state so that all the Mg introduced for spheroidization has faded. In these graphs, the vertical dashed line indicates the calculated temperature for the stable eutectic. It is seen that the records show one main peak associated to the eutectic reaction, and a much smaller thermal arrest at higher temperatures. Comparison of the peaks associated to the eutectic reaction in Figures 3-a for with-CHG and 3-b for no-CHG materials shows that the DTA records on both materials are similar whatever the cooling rate, from 2.5 to 20ºK/min. As a matter of fact, the change in the cooling rate

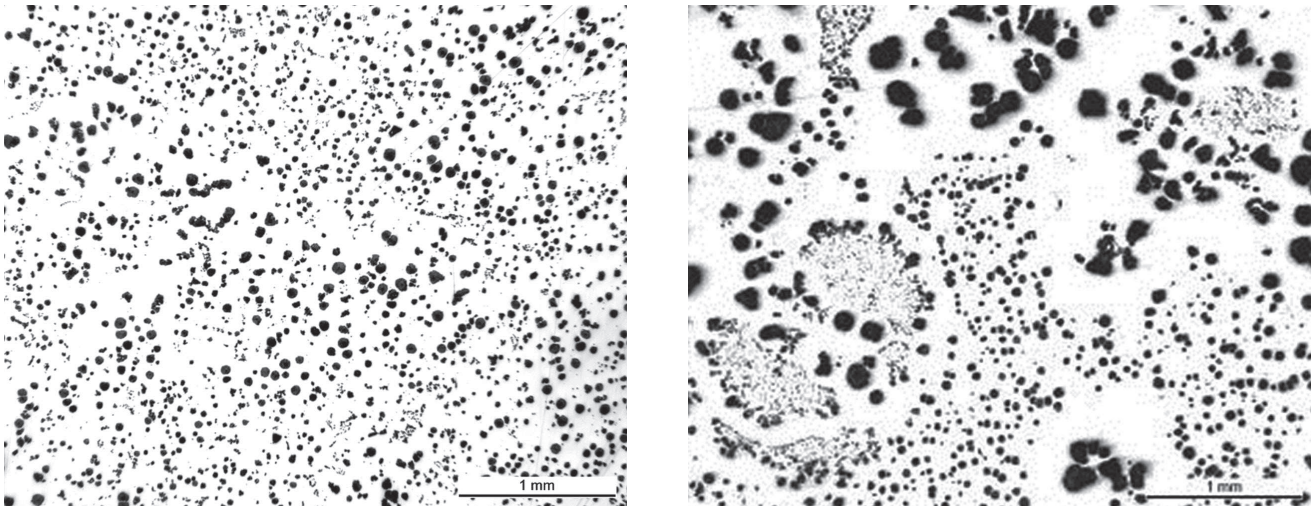

(a) *(b)*

Figure 2. Optical micrographs of the cast material taken (a) in the non-affected outer area and (b) in the central part of the block.

effects similarly undercooling for the onset of the eutectic reaction and the shape of the eutectic arrest of both the with-CHG and no-CHG materials.

The micrographs in Figure 4 show the microstructure of both materials after cooling at 10ºK/min. where it is observed that solidification led effectively to the same microstructure consisting in a lamellar graphite eutectic at the outer surface of the samples which then transforms to undercooled graphite in the central areas. The presence of a significant amount of austenite dendrites allows the peak above the eutectic temperature to be related to primary deposition of austenite, in agreement with the hypoeutectic nature of the alloy. It may be noted in Figure 3 that the start temperature for this peak varies from one sample to another in an "apparently" erratic way, namely apparently without any relationship with the cooling rate or with the material (i.e. with-CHG or no-CHG). A possible explanation could be that the sampling procedure for machining DTA samples induced slight change in the actual carbon content from one sample to another. Such a difference would lead to a change in the observed liquidus temperature without affecting the eutectic reaction itself. Such a sensitivity to sampling may simply be related to the fact that the characteristic size of the microstructure in the blocks, either austenite dendrites or CHG cells, is of the same order as the size of the blanks used for DTA.

A further comparison of the microstructure obtained after a DTA run is given in Figure 5 for samples solidified at 2.5ºK/min. It is seen that lamellar graphite shows the same features for both with-CHG and no-CHG materials mainly consisting of coarse graphite lamellae. This change in the graphite morphology with respect to Figure 4 is a consequence of the reduction in the cooling rate and thus in the graphite growth rate from liquid.

In Figure 6 we compare the DTA traces recorded during the first and second coolings of the additional trial carried out for the no-CHG material. The vertical interrupted line represents, as before, the calculated stable eutectic temperature. The main differences between these two records show up during the eutectic reaction, which consists of two and one peaks for the first and second cooling records respectively. The same behaviour was observed for the with-CHG material. It is noteworthy that the first eutectic peak during the first cooling starts at nearly the same temperature as the single eutectic peak during the second cooling. This suggests relating it to an initial eutectic solidification with lamellar graphite also for the first cooling. However, after this short initial transformation, the main eutectic reaction during the first cooling takes place at a much higher undercooling that is more typical of compacted-vermicular (CVG) or spheroidal (SG) graphite.

The graphs in Figure 7 compare the DTA curves recorded for various cooling rates on with-CHG (solid lines) and no-CHG (dotted lines) materials after a very short stay in the liquid state. In these graphs, the reference line corresponding to the stable eutectic temperature has been superimposed as shown in Figure 3. The corresponding microstructures are illustrated in Figure 8. Looking first at the records obtained with no-CHG samples (dotted lines in Figure 7), it is seen that they all show the same features for the eutectic reaction, i.e. a small peak starting at about the stable eutectic temperature and a main peak at significant undercooling. The microscopic observations showed effectively very little lamellar graphite as illustrated in Figure 8 (column to the right) and the bulk material has solidified with a mix of vermicular and spheroidal graphite.

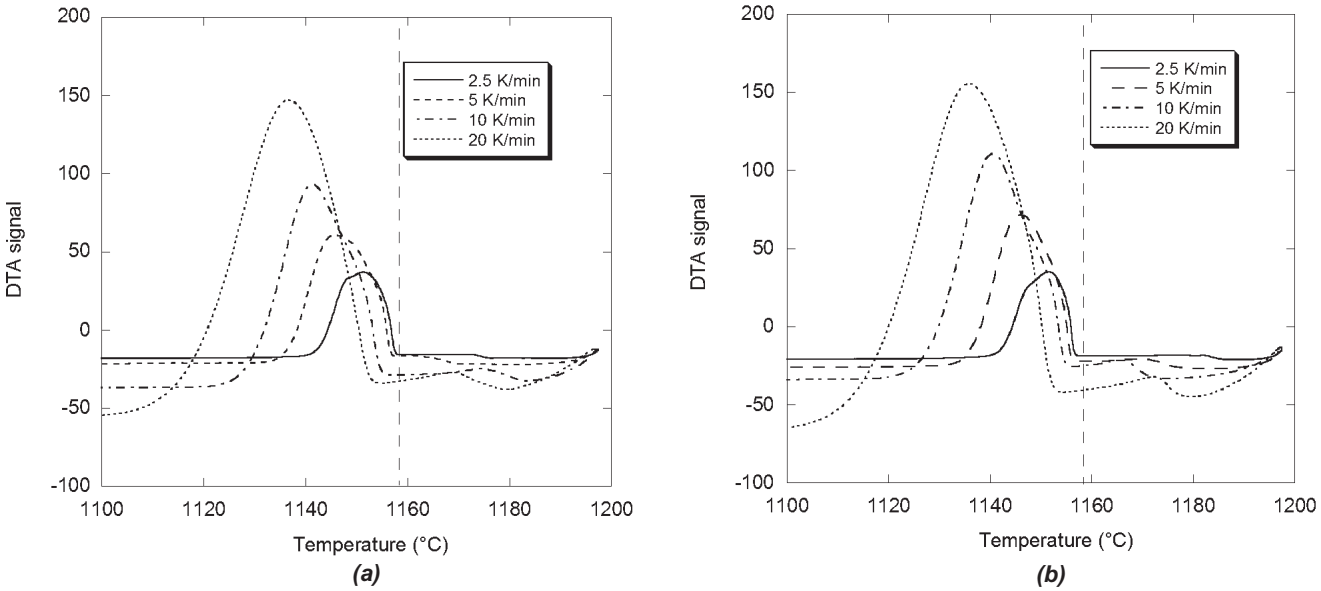

Figure 3. Effect of cooling rate on solidification of (a) with-CHG and (b) no-CHG materials after holding at 1200°C to eliminate Mg. The vertical dashed line represents the calculated eutectic temperature.

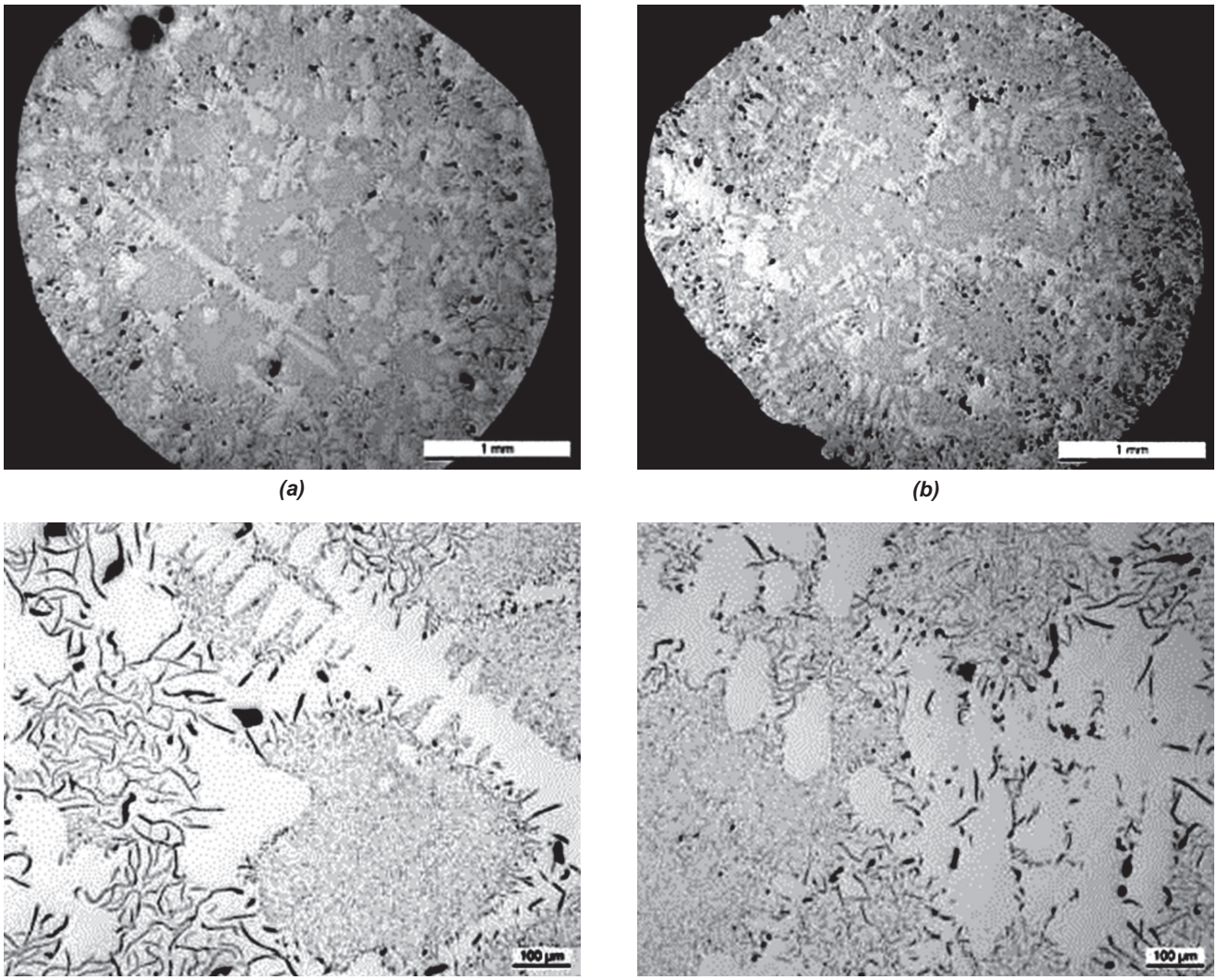

(a) *(b)*

(c) *(d)*

Figure 4. Micrographs of with-CHG (a and c) and no-CHG (b and d) DTA samples after melting at 1200°C, holding for 1800 s and cooling at 10 K/min. Micrographs c and d were taken at the limit between the outer lamellar zone and the inner undercooled area.

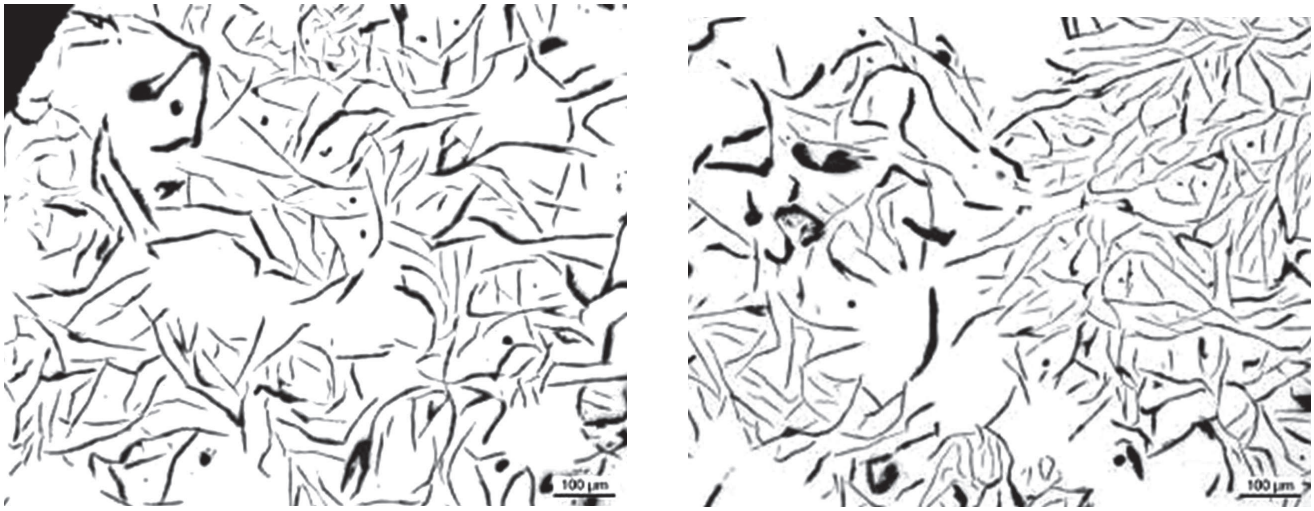

(a) *(b)*

Figure 5. Micrographs of (a) the with-CHG and (b) no-CHG DTA samples after cooling at 2.5 K/min.

In contrast with the DTA records obtained from the no-CHG material, those obtained for with-CHG show features apparently varying with the cooling rate. Considering firstly the records for the slower and higher cooling rates for the with-CHG material, it is seen they appear similar to those for the no-CHG material, though extended over a slightly larger temperature range. Comparing the corresponding microstructures illustrated in Figure 8 (column to the left), it is noted that the with-CHG samples present a higher number of nodules than no-CHG samples. For the intermediate cooling rate of 10ºK/min, the DTA record on the with-CHG material also shows two peaks during the eutectic reaction, but in this case of similar amplitude (in contrast with all other records). Looking at the corresponding micrograph in Figure 8 (note that the scale is not the same as for the other samples), it is seen that these two peaks may be easily associated with a two-step solidification of the sample, the outer shell with lamellar (undercooled) eutectic and the inner part with nodular/vermicular eutectic. As for the other cooling rates, it should be stressed that the nodule count in the central area is much higher for the with-CHG material than for no-CHG.

The reproducibility of the DTA traces recorded at a cooling rate of 10ºK/min was checked with the additional trial mentioned previously. For both the with-CHG and no-CHG materials, it was found that the record for the first cooling was similar to that after rapid melting and immediate cooling, while the second record after holding was similar to the one of the first series of DTA runs which includes a high temperature holding. This underlines the peculiarity related to the 10ºK/min cooling rate, namely that the difference of the DTA records for with-CHG and no-CHG materials at that particular cooling rate, is reproducible.

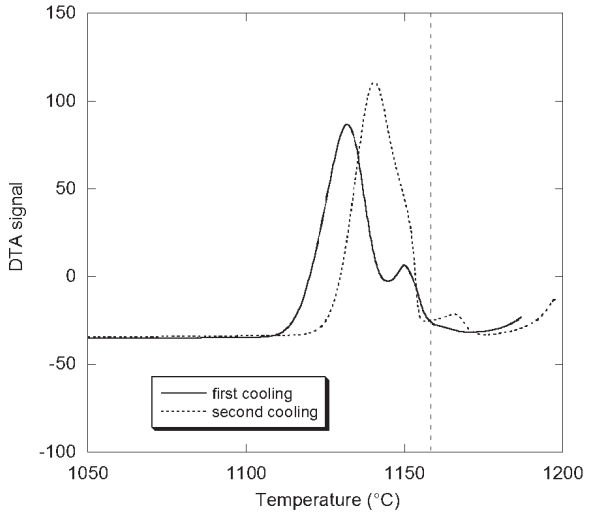

Figure 6. Comparison of the DTA traces recorded during the first and second coolings of the additional trial in the case of the no-CHG material. The vertical dashed line represents the calculated temperature of the stable eutectic.

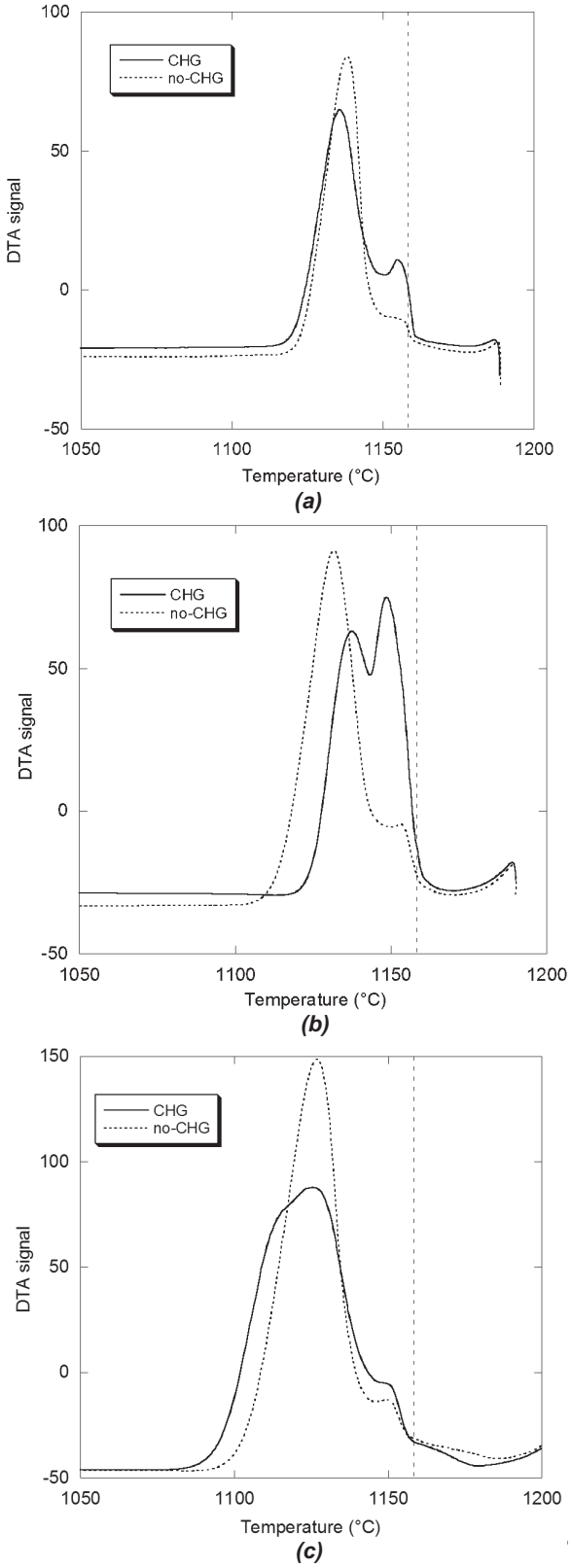

Figure 7. Comparison of the DTA records obtained upon cooling of with-CHG (solid lines) and no-CHG (dotted lines) materials after very short holding in the liquid state. Cooling rates were (a) 5 K/min, (b) 10 K/min and (c) 15 K/min. The vertical dashed line represents the calculated eutectic temperature.

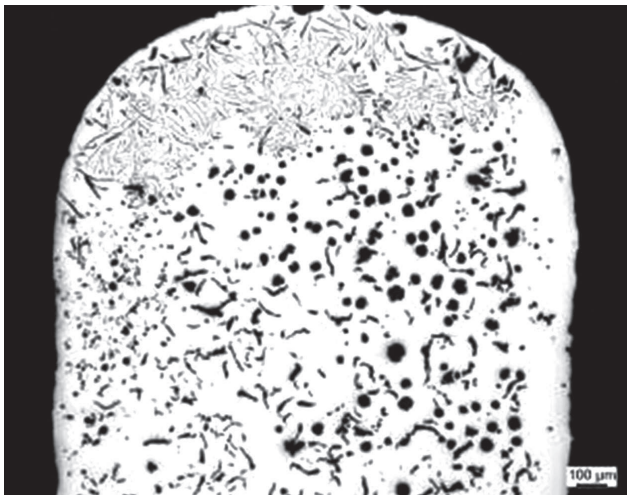

(a) with-CHG

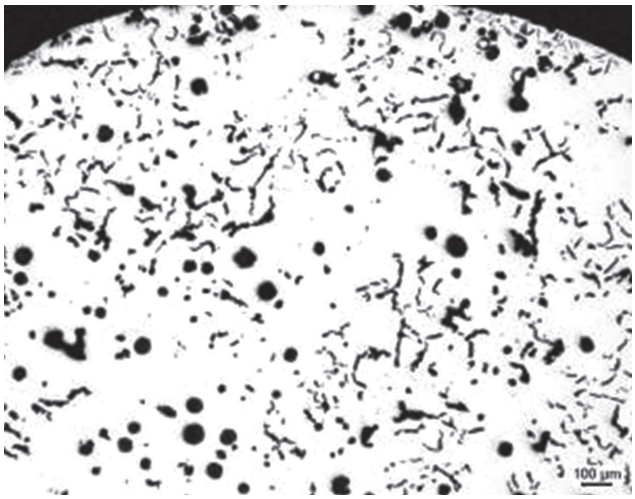

(a) no-CHG

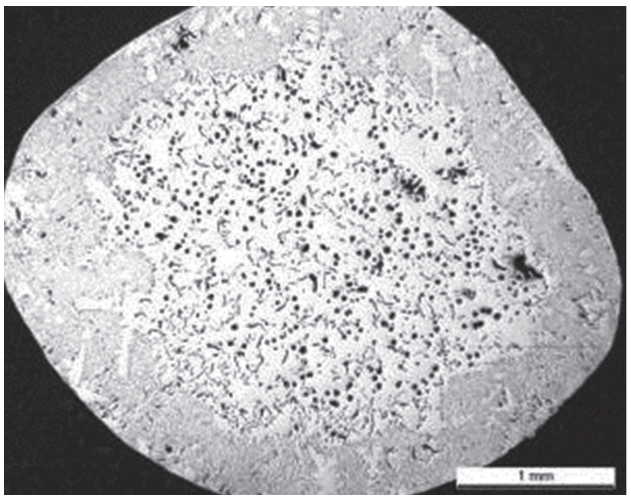

(b) with-CHG

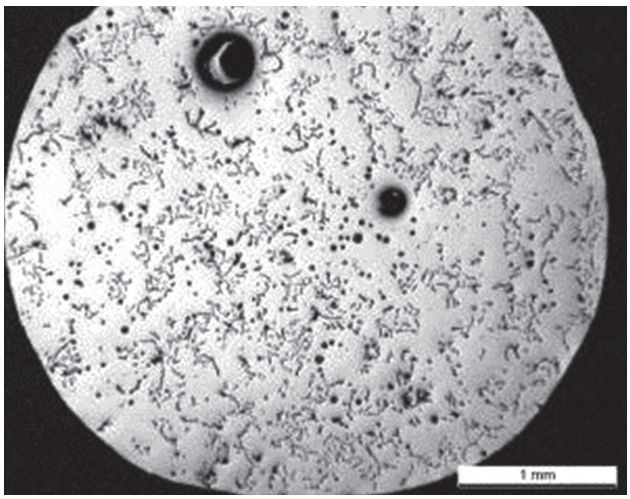

(b) no-CHG

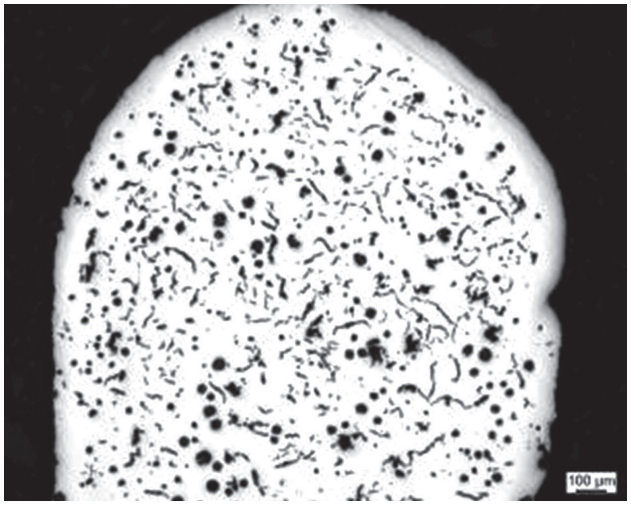

(c) with-CHG

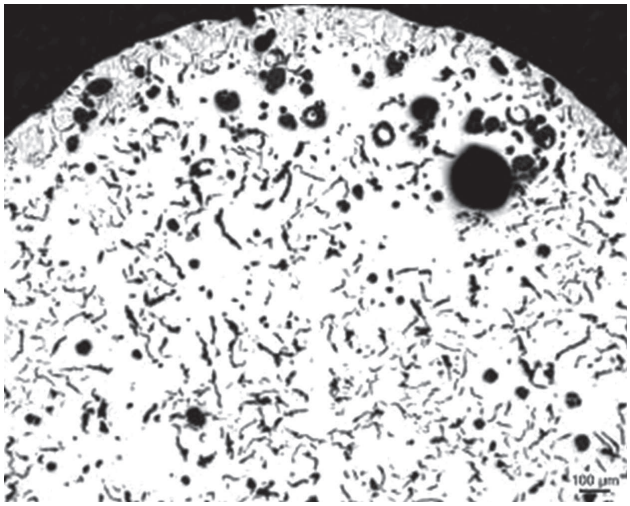

(c) no-CHG

Figure 8. Micrographs of the DTA samples from the with-CHG and no-CHG areas cooled at various scanning rates: (a) 5 K/min, (b) 10 K/min and (c) 15 K/min. Note that the scale is not the same for (b) with-CHG and (b) no-CHG as for the other micrographs.

Discussion

The higher nodule count observed in re-solidified material from the with-CHG areas as compared to no-CHG samples is considered to be due to metallurgical differences between the materials. As no significant chemical heterogeneities are expected,[8-11] this suggests that elements such as magnesium that favour spheroidal growth got bound as compounds in the with-CHG area when the block solidified. This could be in line with the observation of Källbom et al.[9] who noticed the presence of numerous inclusions in the heavy section castings they studied, that contain Mg and S but not O in the chunky cells, while in areas with spheroidal graphite and at the with-CHG cell borders particles containing Mg, O and Si were observed. The fact that the solidification behaviour of with-CHG and no-CHG materials is identical after the melt has been held for some time at 1200C (2192F) suggests that the precipitates considered above appear below 1200C (2192F) during the slow cooling of heavy section castings. A tentative schematic of metallurgical evolution during DTA experiments could be that remelting the material led to immediate volatilization of magnesium in the case of no-CHG material, while this step was preceded by the dissolution of the compounds in the case of with-CHG material. This extra time gave rise to a higher level of magnesium available during re-solidification of with-CHG samples than of the no-CHG ones, thus explaining that more spheroidal graphite was observed in the former. The sensitivity of the DTA records to the cooling rate in the case of the with-CHG material should thus be related to time-dependent dissolution/precipitation processes of compounds in the liquid cast iron.

Conclusion

After holding the with-CHG and no-CHG materials in the liquid state long enough for them to be freed of any nodularizing element, their solidification proceeds similarly by deposition of a coupled eutectic with lamellar or undercooled graphite. The eutectic reaction starts with similar and low undercooling with respect to the stable eutectic temperature, and no significant change in the rate of growth could be detected from the DTA curves which could be related to the change from lamellar to undercooled graphite.

When the material is kept for a very short period in the liquid state before cooling, solidification starts again with lamellar graphite but then this reaction slows down until a high enough undercooling is reached when spheroidal and vermicular graphite may grow. Re-solidification of with-CHG material gives rise to a higher nodule count than no-CHG material, and this suggests that nodularizing elements become bound in compounds during the lengthy eutectic solidification period of heavy-section cast blocks. While this does not give rise to any overall chemical heterogeneity when comparing with-CHG and no-CHG areas, the process does affect the amount of nodularizing elements actually available in the remaining liquid. The exact process and the nature of the compounds involved are still to be investigated.

Acknowledgements

The authors would like to thank the financial support obtained from the Industry Department of the Spanish Government for (ref. PROFIT FIT-030000-2007-94).

REFERENCES

1. Elliott, R., *Cast Iron Technology*, Butterworths (1988).
2. Javaid, A., Loper, C.R., "Production of Heavy-Section Ductile Cast Iron," *AFS Transactions*, vol. 103, pp. 135-150 (1995).
3. Karsay, S.I., "Control of Graphite Structure in Heavy Ductile Iron Castings," *AFS Transactions*, vol. 78, pp. 85-92 (1970).
4. Strizik, P., Jeglitsch, F., "Contribution to the Mechanism of Formation of Chunky Graphite," *AFS International Cast Metals Journal*, vol. 1, pp. 23-30 (1976).
5. Liu, P.C., Li, C.L., Wu, D.H., Loper, C.R., "SEM Study of Chunky Graphite in Heavy Section Ductile Iron", *AFS Transactions*, vol. 91, pp 119-126 (1983).
6. Asenjo, I., Lacaze, J., Larrañaga, P., Méndez, S., Sertucha, J., Suárez, R., "Microstructure Investigation of Small-Section Nodular Iron Castings with Chunky Graphite," *Key Engineering Materials*, vol. 457, pp. 52-57 (2011).
7. Gagné, M., Labrecque, C., Javaid, A.,"Effects of Wall Thickness on the Graphite Morphology and Properties of D5-S Austenitic Ductile Iron," *AFS Transactions*, vol. 115, pp. 411-421 (2007).
8. Gagné, M., Argo, D., "Heavy Section Ductile Iron Castings – Part I: Structure and Properties," Proceedings of the International Conference, *Advanced Casting Technology*, Easwaren J. ed., ASM Int., pp. 231-256 (1987).
9. Källbom, R., Hamberg, K., Björkegren, L.-E., "Chunky Graphite in Ductile Iron Castings," *World Foundry Congress*, paper 184 (2006).
10. Prinz, B., Reifferscheid, K.J., Schulze, T., Döpp, R., Schürmann, E., "Investigation of Causes of Graphite Degenerations of SG Iron like Chunky Graphite," *Giessereiforschung*, vol. 43, pp. 107-115 (1991).
11. Mendez, S., Lopez, D., Asenjo, I., Larranaga, P., Lacaze, J., "Improved Analytical Method for Chemical Analysis of Cast Irons Application to Castings with Chunky Graphite," *ISIJ International*, vol. 51, pp. 242-249 (2011).
12. Asenjo, I., Larrañaga, P., Sertucha, J., Suarez, R., Gomez, J.-M., Ferrer, I., Lacaze, J., "Effect of Mould Inoculation on the Formation of Chunky Graphite in Heavy-Section Spheroidal Graphite Cast Iron Parts," *International Journal of Cast Metals Research*, vol. 20, pp. 319-324 (2007).
13. Castro, M., Herrera, M., Cisneros, M.M., Lesoult, G., Lacaze, J., "Simulation of Thermal Analysis Applied to the Description of the Solidification of Hypereutectic SG Cast Irons," *International Journal of Cast Metals Research*, vol. 11, pp. 369-374 (1999).

Technical Review & Discussion

Experimental Evidence for Metallurgical Modification Associated to Chunky Graphite in Heavy-Section Ductile Iron Castings

J. Lacaze; CIRIMAT, Université de Toulouse, Toulouse, France; I. Asenjo, S. Méndez, J. Sertucha, P. Larrañaga, R. Suárez; Engineering and Foundry Department, Azterlan, Durango (Bizkaia), Spain

Reviewer: The chunky graphite problem has had many papers published which have related the formation of chunky to the presence of cerium. I wonder if the authors have considered that compounds of cerium, not compound of magnesium could be what is removed by extended holding? Free cerium could also act to form nodules.

Authors: *We do agree that other elements may play a role, as noted in the beginning of the discussion section. The emphasis was put on magnesium because it is by far the main spheroidizing element in the investigated alloy.*

Reviewer: The authors only reference one thermal analysis paper; many have been previously published that appear to explain the data quite nicely. Secondly, phase transformation temperatures are known to be a function of cooling rate.

Authors: *The paper dealing with thermal analysis was referenced only because it contains the information for calculating the stable eutectic temperature. The effect of cooling rate on the characteristics of cooling curves obtained by thermal analysis or differential thermal analysis is effectively so well known that it did not appear necessary to elaborate on that. The curves were shown for comparison purpose, namely discussing the similarities and differences obtained with CHG (now called "with-CHG") and no-CHG materials.*

Reviewer: The authors should document how they "calculated" the eutectic temperature (they would need to know the composition of both the CHG and no-CHG regions in the sample to do so) and whether or not they tried to account for the effect of cooling rate on the eutectic temperature.

Authors: *The composition of the cast-iron is given in the section "experimental details", and it has been verified that it is the same in the CHG and the no-CHG areas (reference #11), i.e. that there is no macrosegregation. The eutectic temperature which is evaluated is that obtained from a phase diagram calculation, denoted "stable eutectic temperature" just above, as described in reference #13. Its value is given in the same paragraph of the section "experimental details".*

Reviewer: The data shown in Figure 3 looks like classic nucleation and growth.

Authors: *Certainly, and the stable eutectic temperature gives the upper temperature limit for both nucleation and growth.*

Reviewer: The DTA records that show two phase transformations (Figs 6&7) may simply be a liquidus and solidus-the recalescence that occurs due to undercooling or differences in inoculation. The reported chemistry is near eutectic and the authors did not determine the actual chemistry of their DTA samples. This needs to be clarified.

Authors: *It may be necessary to stress that DTA is not obtained by differentiating a thermal analysis curve. Any peaks on a DTA record such as the two peaks appearing in the eutectic range of this study relate to heat release in the sample. Accordingly, the solidus that is the end of solidification, would not give a peak, though it may possibly be associated to a peak summit.*